JOC The Journal of Organic Chemistry

Article

pubs.acs.org/joc

Structural Refinement of Ladder-Type Perylenediimide Dimers: A Classical Tale of Conformational Dynamics

Mykhaylo Myahkostupov,[†,§] Valentina Prusakova,[†,§] Daniel G. Oblinsky,[‡] Gregory D. Scholes,[‡] and Felix N. Castellano*[,†,#]

[†]Center for Photochemical Sciences and Department of Chemistry, Bowling Green State University, Bowling Green, Ohio 43403, United States

[‡]Department of Chemistry, Institute for Optical Sciences, and Centre for Quantum Information and Quantum Control, University of Toronto, Toronto, Ontario, M5S 3H6, Canada

Supporting Information

ABSTRACT: We have synthesized and thoroughly characterized two representative ladder-type acetylene-bridged perylenediimide dimers bearing long alkyl chain solubilizing groups, bis[1-ethynyl-*N*,*N*′-bis(1-hexylheptyl)-perylene-3,4:9,10-tetracarboxylic diimide] ([PDICC]$_2$, **1**) and 1,1′-ethynyl-bis[*N*,*N*′-bis(1-hexylheptyl)-perylene-3,4:9,10-tetracarboxylic diimide] ([PDI]$_2$CC, **2**). In these dimeric PDI molecules, NMR-based structural characterization became nontrivial because severe ^{1}H spectral broadening and greater than expected numbers of observed ^{13}C resonances substantially complicated the interpretation of traditional 1-D spectra. However, rational two-dimensional NMR approaches based on both homo- and heteronuclear couplings (^{1}H−^{1}H COSY; ^{1}H−^{13}C HSQC), in conjunction with high-level structural DFT calculations (GIAO/B3LYP/6-31G(d,p)/PCM, chloroform), were readily applied to these structures, producing well-defined analytical characterization, and the associated methodology is described in detail. Furthermore, on the basis of dynamic NMR experiments, both **1** and **2** were found to exist in a perylene-centered conformational dynamic equilibrium ($\Delta G‡$ = 13−17 kcal/mol), which primarily caused the observed ambiguities in conventional 1-D spectra.

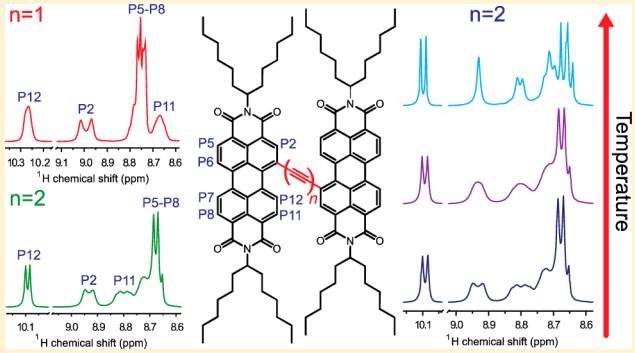

INTRODUCTION

For quite some time, perylenediimides (PDIs) have attracted substantial scientific interest thanks to their unique set of chemical, photochemical, and photophysical properties.[1−6] In particular, PDIs coupled to other chromophoric species have been considered excellent model systems for gleaning insights into various fundamental and applied aspects of a diverse spectrum of photonic and electronic materials.[7−25] Since PDI functionalization chemistry typically occurs either at the imide site(s) or in the bay region (1-, 6-, 7-, or 12-positions), it allows one to engineer linear or ladder-type multichromophoric PDI-based oligomers with a desired envelope of functional properties.[11,26−33] However, we note that efficient construction of multimeric isomerically pure ladder-type structures is often limited by nontrivial separations of mixtures of 1,6- and 1,7-disubstituted PDIs, although a few successful examples have been reported.[34−37] PDI-based molecular systems are also expected to display solvent programmable propensity toward aggregation, making them ideal candidates for the study of energy and electron transfer processes in both aggregated and nonaggregated forms.[1,2,38−46] Here, we aimed at utilizing highly emissive PDI chromophores as building blocks to construct electronically coupled ladder-type molecular systems that would manifest relatively strong electronic intramolecular interactions and desirable photophysics as a result of being connected through sp-hybridized acetylene bridges. In this case, the extent of electronic coupling can be tuned by varying the number of acetylene bridging units between adjacent PDI chromophoric species. However, any detailed discussion of their associated excited state photochemistry is beyond the scope of the present work and will be a subject of separate contribution.

Oligomeric PDIs bearing short solubilizing alkyl groups (e.g., ethylpropyl) suffer from rather poor solubility in commonly used solvents (such as DCM) and, as a result, achieving sufficient solubility for adequate spectroscopic studies requires the incorporation of higher-order alkyl substituents; for instance, 1-hexylheptyl or cyclohexyl are commonplace.[1,26,35] In support of ongoing research efforts, two representative acetylene-bridged perylenedimide dimers bearing solubilizing 1-hexylheptyl functionalities have been synthesized and thoroughly characterized, bis[1-ethynyl-*N*,*N*′-bis(1-hexylheptyl)-perylene-3,4:9,10-tetracarboxylic diimide] ([PDICC]$_2$, **1**) and 1,1′-ethynyl-bis[*N*,*N*′-bis(1-hexylheptyl)-perylene-3,4:9,10-tetracarboxylic diimide] ([PDI]$_2$CC, **2**), with their corresponding

Received: June 20, 2013
Published: August 13, 2013

 © 2013 American Chemical Society dx.doi.org/10.1021/jo401348w | *J. Org. Chem.* 2013, 78, 8634−8644

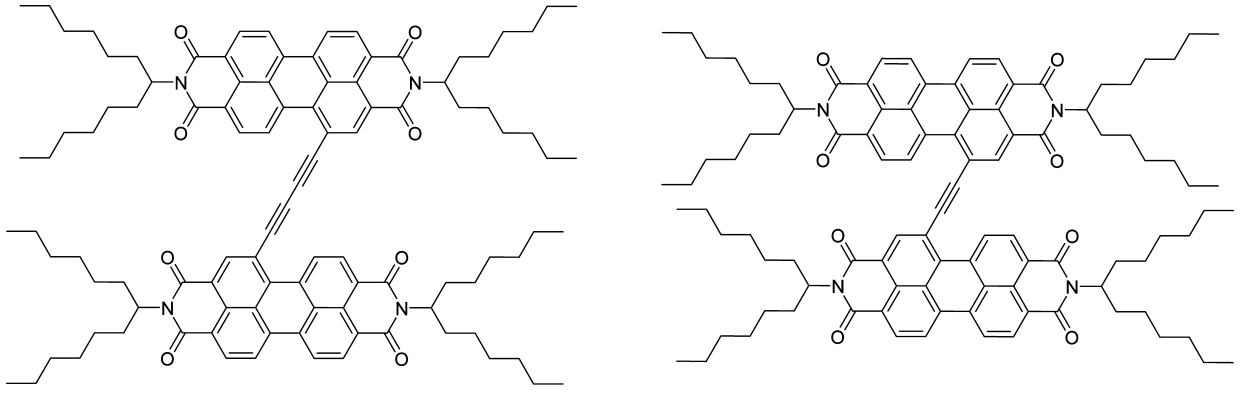

Figure 1. Structures of target ladder-type acetylene-bridged perylenediimide dimers: $[PDICC]_2$ **1** (left) and $[PDI]_2CC$ **2** (right). The corresponding synthetic scheme is presented in Supporting Information Figure S1.

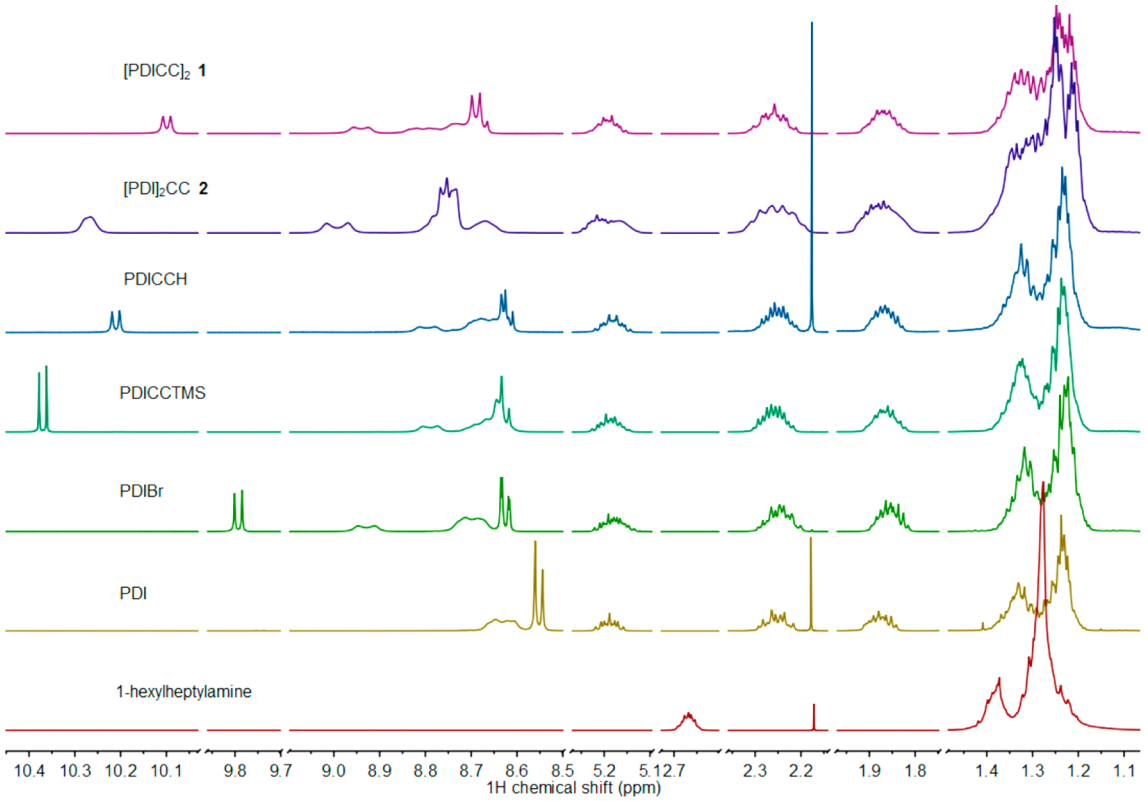

Figure 2. The evolution of ^1H NMR spectra (500 MHz, $CDCl_3$, 300 K) in the synthetic sequence toward acetylene-bridged perylenediimide dimers **1** and **2**. For clarity, only the regions of interest are displayed. The representative structures are shown in Figure 1 and the Supporting Information.

chemical structures presented in Figure 1. Although 1-D NMR is typically considered to be sufficient for structural verification in a variety of established PDI-based molecular systems, this was simply not the case in **1** and **2**. Here, multinuclear multidimensional NMR spectroscopy, in conjunction with high-level DFT calculations, was invaluable for the structural refinement of **1** and **2**, and we note that these techniques have been successfully applied to the characterization of many classes of organic and inorganic molecules as well as various biopolymers.[47−52] Given the importance toward understanding the rationale of this approach, the complete structural assignment of **1** (and **2**) using 2-D homo- and heteronuclear correlation NMR spectroscopy is described in detail. Because both **1** and **2** were found to possess very similar structural properties, the bulk of our discussion is primarily dedicated to **1**. In addition, dynamic NMR experiments have been executed to understand the ambiguities associated with single temperature (300 K) 1-D NMR experiments of these PDI dyes.

RESULTS AND DISCUSSION

Structural Refinement of Perylenediimide Dimers. Along with X-ray crystallography, multidimensional high-resolution NMR spectroscopy provides an indispensable and versatile analytical tool for the structural elucidation and assignment of complex organic and organometallic molecules as well as biological macromolecules.[47−51] In addition, NMR

dx.doi.org/10.1021/jo401348w | J. Org. Chem. 2013, 78, 8634−8644

spectroscopy can be uniquely used to probe the structural dynamics at the molecular level while other relevant techniques may fall short in this regard.[53−59] Because of the striking ambiguities observed in 1-D ^{1}H and ^{13}C NMR spectra (measured at 300 K) of synthesized PDI monomeric synthons and target dimers **1** and **2**, such as partial spectral broadening of aromatic ^{1}H resonances (Figure 2) and higher than expected numbers of ^{13}C resonance peaks in proton-decoupled spectra (Supporting Information Figures S2−S4), we performed complete structural assignments using a combination of homo- and heteronuclear (^{1}H, ^{13}C) multidimensional correlation NMR techniques to understand the origin of the observed experimental effects. Furthermore, high level DFT calculations (GIAO/B3LYP/6-31G(d,p)/PCM, chloroform) provided another powerful tool for the computational structural analysis of target PDI molecules, and relevant 1-D ^{1}H NMR chemical shift calculations were performed to support the experimental assignments of proton resonances.[60−62]

Oftentimes, spectral broadening can be a challenging NMR phenomenon to explain, and in terms of related PDI molecular structures, it has been somewhat overlooked in the literature.[26,63,64] In some cases, it was argued that oligomeric PDIs exhibit such behavior as a result of aggregation-induced effects occurring at the applicable NMR sample concentration levels, typically in mM range.[63] In addition, a recent study by Würthner and co-workers demonstrated that dimerized aggregates of monomeric PDI molecules exhibited a pronounced concentration-dependent NMR behavior that was accompanied by the substantial chemical shift changes within the concentration range of 0.02−40.0 mM.[65] However, in the present study, a distinctly different phenomenon has been encountered. As demonstrated here for monomeric PDICCTMS (Supporting Information Figure S5), ^{1}H NMR spectra of 1-hexylheptyl-bearing PDIs preserve exactly the same pattern of partial spectral broadening altogether with very minor chemical shift changes within the measured concentration range of 0.2−7.5 mM. Furthermore, the observed spectral broadening appears to be characteristic of 1-hexylheptyl-bearing perylenediimides only, whereas no such broadening was observed for PDIs incorporating other alkyl substituents, such as ethylpropyl[66] or dicyclohexylmethyl (data not shown), at comparable concentration levels. As we found in the present work, an intrinsically different mechanism becomes a major player here: a PDI molecule bearing 1-hexylheptyl substituents turns out to be very dynamic on NMR time scales (typically, 10^{-3}−10^{0} s range)[57] and is the subject of detailed discussion below. We also note here that splitting pattern in the aliphatic regions of 1-D ^{1}H NMR spectrum changes dramatically once the PDI molecule is completely formed (Figure 2), and this effect will be thoroughly discussed, as well.

Since both monomeric and dimeric PDIs were found to display similar NMR behavior (see the Supporting Information), we selected PDI dimer **1** as a representative example for further comprehensive discussion. To facilitate the interpretation and assignment of the obtained 2-D NMR data, the structural aspects of **1** were labeled and color-coded according to the scheme presented in Figure 3 and are explicitly applicable to all other PDI molecules mentioned in the present study. We note that **1** (and **2**) bear identical perylenediimide−acetylene moieties that remain nearly equivalent within the same molecular framework in terms of NMR spectroscopic behavior. As a result, **1** (and **2**) can be rendered as "monomer-like" on the basis of the profound similarities of their 1-D and

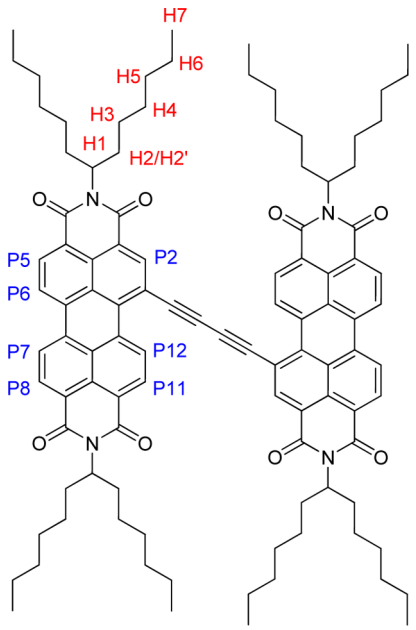

Figure 3. Labeling scheme for the structural assignment of acetylene-bridged PDI dimers. $[PDICC]_2$ **1** is shown as a representative example.

2-D NMR spectra with those of PDI monomeric synthons (Figures 2, 4, 6, 8, and Supporting Information S6−S12). Thus, we will focus our attention only on the characterization of a single PDI fragment within the molecular framework of **1** (Figure 3). Since the assignment of quaternary carbons would not result in any meaningful improvements of overall structural refinement of **1** (and **2**), these were purposely omitted. All protons have been assigned on the basis of ^{1}H−^{1}H correlation COSY experiments, whereas proton-attached carbons have been assigned via ^{1}H−^{13}C correlation HSQC experiments, respectively (Figures 4, 6, 8, and Supporting Information S6−S14). For both **1** and **2**, all structurally assigned ^{1}H and proton-attached ^{13}C resonances are summarized in Table 1. We also note that both homo- (^{1}H−^{1}H) and heteronuclear (^{1}H−^{13}C) correlations were necessitated because proper assignments could not be accomplished solely on the basis of ^{1}H−^{1}H correlations. The details of the most important steps encountered during the structural assignment of **1** are given below.

On the basis of the obtained NMR data, the PDI molecule possesses two characteristically distinct spin systems (the aromatic perylene core (P2−P12) and the aliphatic 1-hexylheptyl group (H1−H7)) that behave independently of each other in terms of 2-D NMR spectroscopy. As such, they will be discussed separately for clarity, starting with the assignment of ^{1}H and ^{13}C resonances in the aliphatic regions. We first note that the aliphatic 1-hexylheptyl group remains pseudosymmetric, even when the perylene core symmetry is broken as a result of the introduction of a substituent in the 1-position of its bay region. The proton (δ 5.23−5.15 ppm, Table 1) and carbon (δ 54.98; 54.79 ppm, Table 1) resonances attributed to the H1 position (next to imide nitrogen) are characteristic of a wide variety of perylenediimide molecules in general and, consequently, can be used as reference points. On the basis of the ^{1}H−^{1}H COSY experiment (Figure 4), the H1 proton was found to correlate with two adjacent protons (H2 and H2′), all within three covalent bonds, whereas the ^{1}H−^{13}C

dx.doi.org/10.1021/jo401348w | J. Org. Chem. 2013, 78, 8634−8644

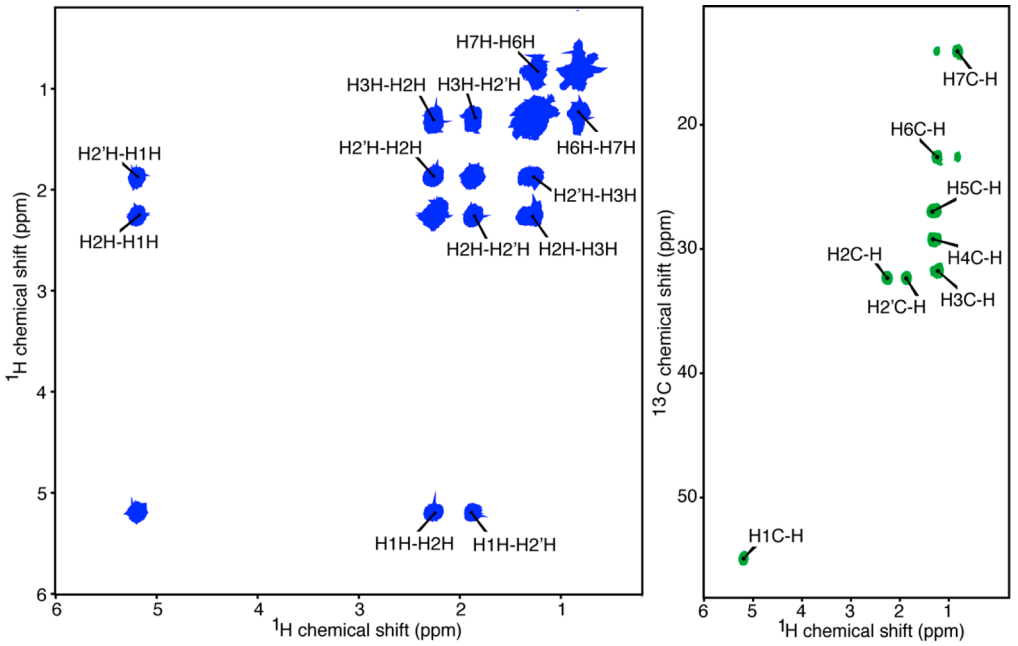

Figure 4. Selected aliphatic regions of 2-D NMR correlation spectra (500 MHz, $CDCl_3$, 300 K) of **1** with complete peak assignments: ^{1}H−^{1}H COSY (left, blue colored) and ^{1}H−^{13}C HSQC (right, green colored). The labeling scheme is presented in Figure 3.

Table 1. Complete Structural Assignment of PDI Dimers 1 and 2 Based on 1-D and 2-D NMR Data Acquired at 300 K[a]

	[PDICC]$_2$ (**1**)		[PDI]$_2$CC (**2**)	
atom no.	^{1}H (ppm)	^{13}C (ppm)	^{1}H (ppm)	^{13}C (ppm)
H1	5.23−5.15	54.98; 54.79	5.25−5.16	55.03; 54.79
H2	2.30−2.21	32.33	2.31−2.19	32.34
H2′	1.90−1.83	32.33	1.92−1.86	32.34
H3	1.38−1.21	31.78; 31.75	1.36−1.20	31.78; 31.74
H4	1.38−1.21	29.23; 29.22	1.36−1.20	29.24; 29.22
H5	1.38−1.21	26.92	1.36−1.20	26.95; 26.91
H6	1.38−1.21	22.61; 22.59	1.36−1.20	22.62; 22.59
H7	0.84; 0.81	14.07; 14.05	0.84; 0.81	14.07; 14.04
P2	8.96−8.92	139.25; 138.58	9.01−8.97	138.13; 137.53
P5	8.74−8.66	131.18; 130.79	8.78−8.66	131.50; 130.99
P6	8.74−8.66	123.69; 123.38	8.78−8.66	123.84; 123.42
P7	8.74−8.66	131.54; 131.18	8.78−8.66	131.70
P8	8.74−8.66	132.28; 131.93	8.78−8.66	132.26
P11	8.82−8.79	131.93; 131.18	8.69−8.66	131.70; 131.1
P12	10.10	127.22; 126.89	10.27	127.47

[a]The representative labeling scheme is shown in Figure 3.

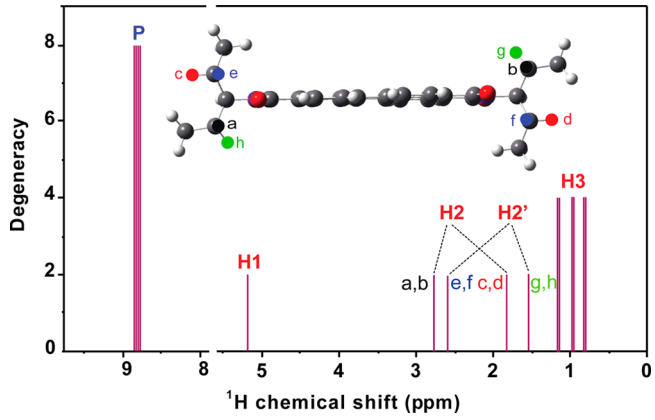

Figure 5. Calculated DFT GIAO 1-D ^{1}H NMR spectrum of $(C_5)_2$PDI in a chloroform solvent continuum (PCM) using B3LYP functional and 6-31G(d,p) basis set. For clarity, the labeled lowest-energy ground state geometry structure is presented. The internal dihedral angle formed around the central six-member ring was calculated to be <2°.

HSQC experiment revealed that both H2 (δ 2.30−2.21 ppm, Table 1) and H2′ (δ 1.90−1.83 ppm, Table 1) protons are attached to the same carbon (δ 32.33 ppm, Table 1), as evidenced by the appearance of two equally intense, equal ^{13}C chemical shift cross-peaks (Figure 4). As supported by DFT calculations (Figure 5), protons H2 and H2′ become diastereotopic when the PDI molecule is fully assembled, thus resulting in their substantial (~0.4 ppm) chemical shift difference (Figure 8, Table 1). Interestingly, this effect is completely absent in 1-hexylheptylamine and becomes apparent only when the PDI molecule is constructed (Figure 2). Furthermore, it is important to note that the observed H2−H2′ proton splitting is quite universal and is consistently conserved in the entire series of investigated PDI molecules, including those bearing ethylpropyl substituents (see Supporting Information) and, to the best of our knowledge, has not yet been recognized in the literature.

All other aliphatic protons and carbons were found to exhibit rather typical hydrocarbon behavior and were assigned on the basis of their remoteness from the imide group, that is, distancing away from the imide group causes an increasingly upfield chemical shift (Table 1). All remaining carbons (H3−H6 and H7) produced well-resolved single ^{1}H−^{13}C HSQC cross-peaks that were assigned in a straightforward manner (Figure 4, Table 1). On the other hand, their corresponding ^{1}H resonances (H3−H6) were found to fall within the same broad multiplet (δ 1.38−1.21 ppm, Table 1, Figures 4 and 8) and, thus, were very difficult to differentiate. In turn, the methyl protons at the H7 end group produced an easily assignable set of two overlapping triplets (δ 0.84, 0.81 ppm; Table 1).

To support the experimental NMR observations of H2−H2′ proton splitting, DFT 1-D ^{1}H NMR calculations of the model

dx.doi.org/10.1021/jo401348w | J. Org. Chem. 2013, 78, 8634−8644

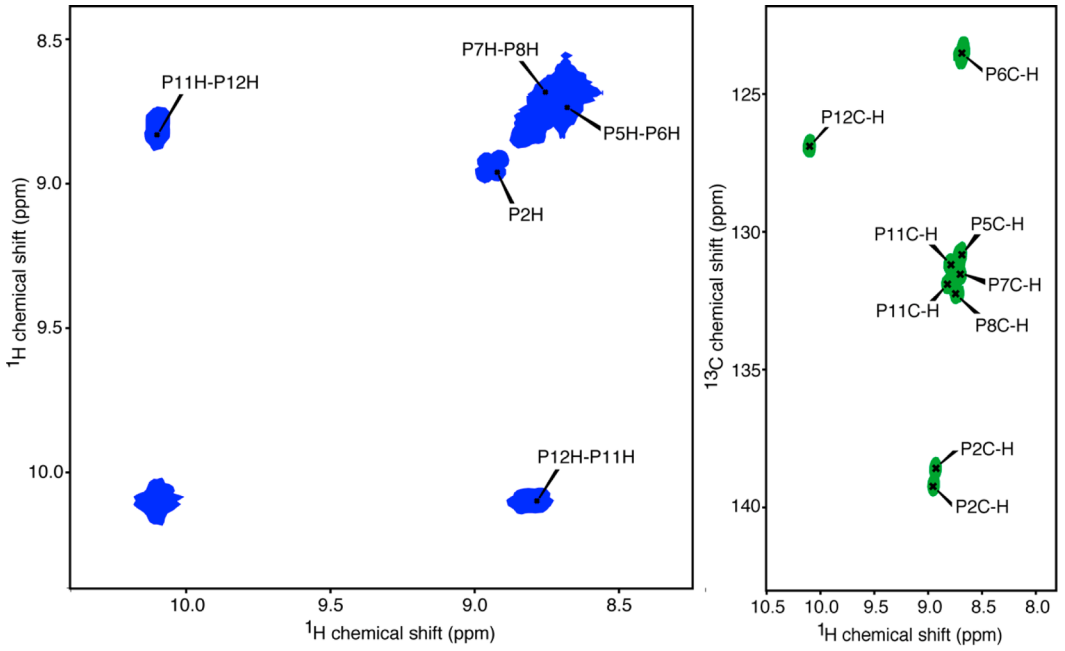

Figure 6. Selected aromatic regions of NMR correlation spectra (500 MHz, $CDCl_3$, 300 K) of **1** with complete peak assignments: ^{1}H−^{1}H COSY (left, blue) and ^{1}H−^{13}C HSQC (right, green). The labeling scheme is presented in Figure 3.

symmetrical ethylpropyl-bearing $(C_5)_2$PDI compound were performed. As presented in Figure 5, H2 signal arises from a and b, c and d protons that are equal to each other, correspondingly. Moreover, protons a and b appear to be enantiotopic to c and d. Taking into account the free rotation around single C−C bonds, the resulting chemical shift becomes an average of four signals (*a*, *b*, *c*, *d*) and shows excellent agreement with the experimental NMR data (Supporting Information Table S1). The chemical shift behavior of H2′ proton follows exactly the same trend and is a combination of equal contributions from e, f, g, and h protons. Similar to the H2 proton, the calculated chemical shift value of H2′ proton is also in perfect agreement with its experimentally observed values (Supporting Information Table S1). We also note here that the lowest-energy ground state geometry of $(C_5)_2$PDI shows no significant deviation from planarity, with the calculated internal dihedral angle, formed around the central six-member ring, <2° (Figure 5).

The assignment of the aromatic regions proceeded in the following manner. The introduction of acetylene substitution in the 1-position of PDI bay region results in the loss of symmetry within the perylene fragment, and consequently, at 300 K, several sufficiently resolved multiplets in the aromatic regions of ^{1}H NMR spectrum of **1** (and **2**) can be identified (Figures 2, 8, Supporting Information S12). Structurally, these multiplets can be attributed to four different spin systems within the perylene core of **1** (and **2**)—namely P2, P5−P6, P7−P8, and P11−P12—that can be viewed as independent of each other in terms of ^{1}H−^{1}H COSY correlations. It is important to note that the observed aromatic region splitting pattern is indicative of all synthesized monomeric and dimeric PDIs discussed in the present work. The positioning of acetylene group is poised to induce a significant deshielding to its spatially most proximate proton (P12) that appears as the most downfield shifted doublet at δ 10.10 (Figure 8, Table 1). In addition, the experimental assignment of P12 as the most deshielded proton produced excellent agreement with DFT 1-D ^{1}H NMR calculations for dimer **1** and the monomeric model compound (Figures 7 and Supporting Information S15). Since the P12 proton structurally exists in a scalar coupled spin system partnered with the P11 proton (δ 8.82−8.79, Table 1), they generated a symmetric set of corresponding ^{1}H−^{1}H COSY correlation cross-peaks (Figure 6).

As far as the 1-D ^{1}H NMR spectrum of **1** is concerned (measured at 300 K, Figure 8), the P12 proton exhibits a relatively sharp, well-resolved doublet (δ 10.10, J = 8.1 Hz), whereas the P11 proton (δ 8.82−8.79) appears as a severely broadened doublet stemming from conformational dynamics of the perylene aromatic core (see the discussion below). The same dynamic phenomenon is responsible for the broadening and splitting of the P2 proton resonance (δ 8.96−8.92, Figure 8). Structurally, the P2 proton exists as a lone uncoupled nucleus and, as anticipated, does not produce any correlation cross-peaks in the corresponding ^{1}H−^{1}H COSY spectrum (Figure 6). However, its appearance as a pseudodoublet in a conventionally acquired 1-D ^{1}H spectrum can be quite misleading and difficult to interpret because, in reality, it represents a superposition of two broad overlapping singlets still belonging to the same P2 proton that are chemically exchangeable on the NMR time scales. All other aromatic protons (P5−P6 and P7−P8) were contained in an ill-defined chemical shift envelope, rendering it challenging to assign the multiplet at δ 8.74−8.66 (Table 1, Figure 8). Apart from inducing the broadening of the above-mentioned ^{1}H resonances, perylene conformational dynamics is also responsible for the appearance of higher than expected numbers of 1-D ^{13}C peaks (Supporting Information Figures S2−S4) and 2-D C−H cross-correlation peaks in the corresponding ^{1}H−^{13}C HSQC spectra, such as found in P2 and P11 (Figures 6, Supporting Information S8, S11). These experimental findings are consistent with the conformational dynamic behavior that has been recently reported for several bay-substituted macrocyclic PDI monomers.[67]

dx.doi.org/10.1021/jo401348w | J. Org. Chem. 2013, 78, 8634−8644

In addition, DFT 1-D ^{1}H NMR calculations of **1**, $(C_5)_2$PDI and $(C_5)_2$PDICCTMS in a chloroform environment support the relative order of the experimentally observed ^{1}H signals in the aromatic regions (Figures 5, 7, Supporting Information S15). Moreover, the corresponding computed ^{1}H chemical shifts show excellent agreement with the empirically measured values (Supporting Information Tables S1 and S2). Interestingly, on the basis of a comparison of empirical and calculated 1-D ^{1}H NMR spectra of **1** (Figures 7 and 8), its transoid **1A** conformation appears to be a dominant species in solution.

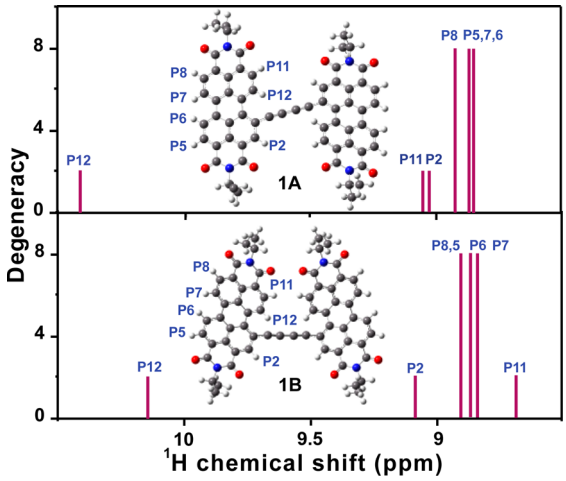

Figure 7. Calculated DFT GIAO 1-D ^{1}H NMR spectra of **1** based on two energy minima, **1A** and **1B** (see Supporting Information Figure S16), in a chloroform solvent continuum (PCM) using the B3LYP functional and 6-31G(d,p) basis set. For clarity, only the aromatic regions are displayed. In addition, the corresponding labeled lowest-energy ground state geometry structures in transoid **1A** (top) and cisoid **1B** (bottom) conformations are presented.

Conformational Dynamics of Perylene Core. To reveal the origin of spectral broadening observed throughout the entire series of synthesized monomeric and dimeric PDIs (Figure 2), we monitored the temperature-dependent behavior of their corresponding ^{1}H NMR spectra in the 300−330 K range (Figures 9, Supporting Information S17−S18), with the upper limit dictated primarily by the physical properties of the solvent of choice ($CDCl_3$). As clearly evident from the elevated temperature-induced changes in the aromatic regions, such as peak sharpening and peak coalescence, both PDI monomers (e.g., PDICCTMS) and dimers (**1** and **2**) exist in a dynamic equilibrium at 300 K arising primarily from the conformational dynamics of the perylene core. On the other hand, the ^{1}H signals in the aliphatic regions (H1−H7, Figures 8-9, Supporting Information S17−S18) were found to undergo very minor temperature-induced changes, and consequently, any possible rotational conformers could not be sufficiently resolved under the employed experimental conditions. It is important to note here that the observed temperature-dependent NMR behavior is fully reversible and does not result from any chemical changes in the sample.

The unique P2 proton (δ 8.96−8.92, Figure 8) is the only uncoupled aromatic proton within the perylene framework and, thus, can serve best to characterize the dynamic behavior of

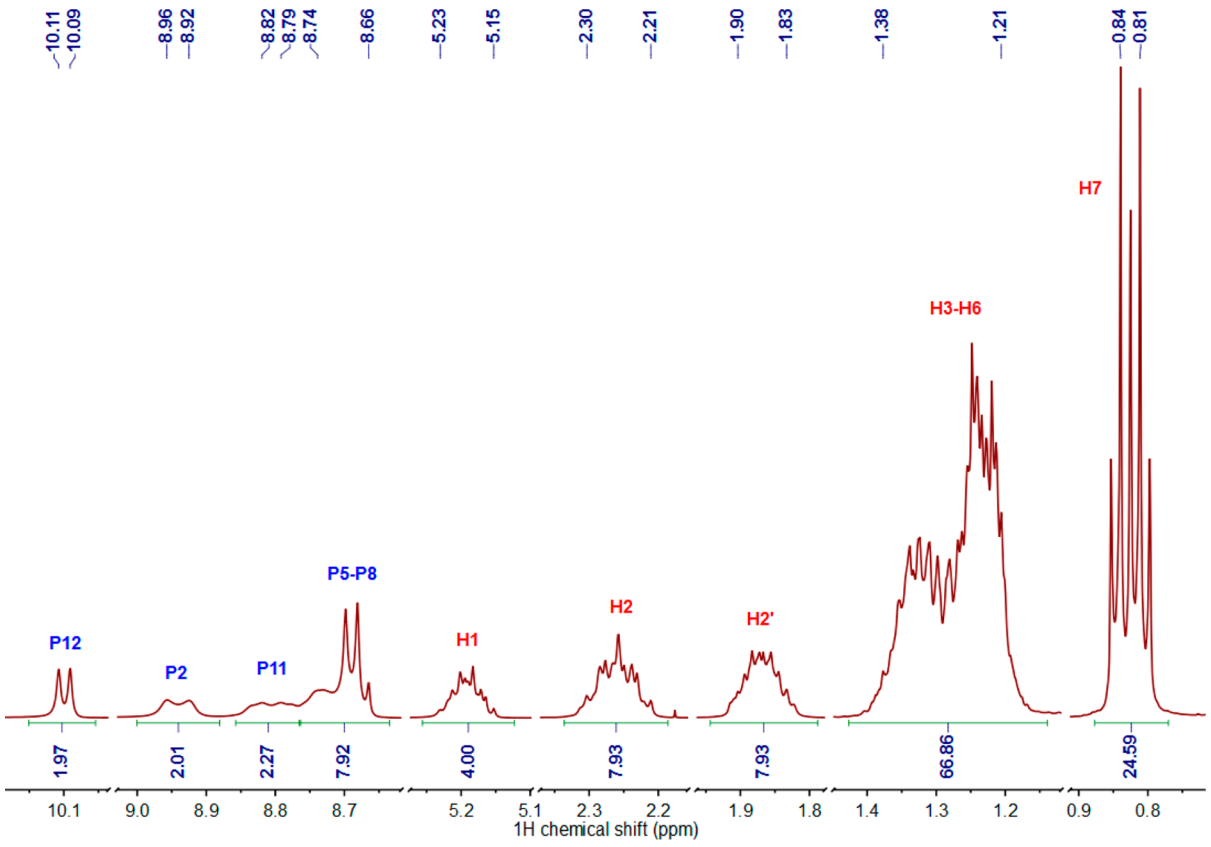

Figure 8. Complete assignment of the 1-D ^{1}H NMR spectrum of **1** (500 MHz, $CDCl_3$, 300 K) using a combination of 2-D NMR data. For clarity, only the regions of interest are displayed. The color- and letter-labeling scheme is presented in Figure 3.

dx.doi.org/10.1021/jo401348w | J. Org. Chem. 2013, 78, 8634−8644

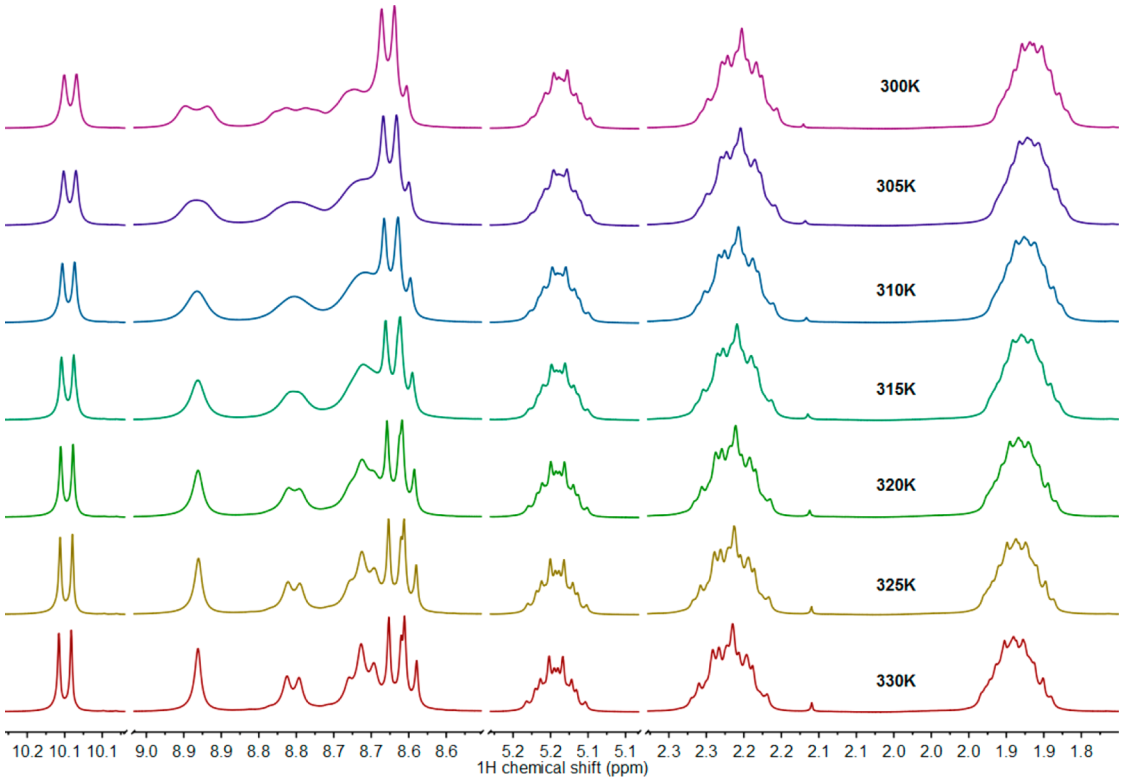

Figure 9. Temperature-dependent 1-D ^{1}H NMR spectra of **1** (500 MHz, $CDCl_3$) measured in the 300−330 K range. For clarity, only the regions of interest are displayed.

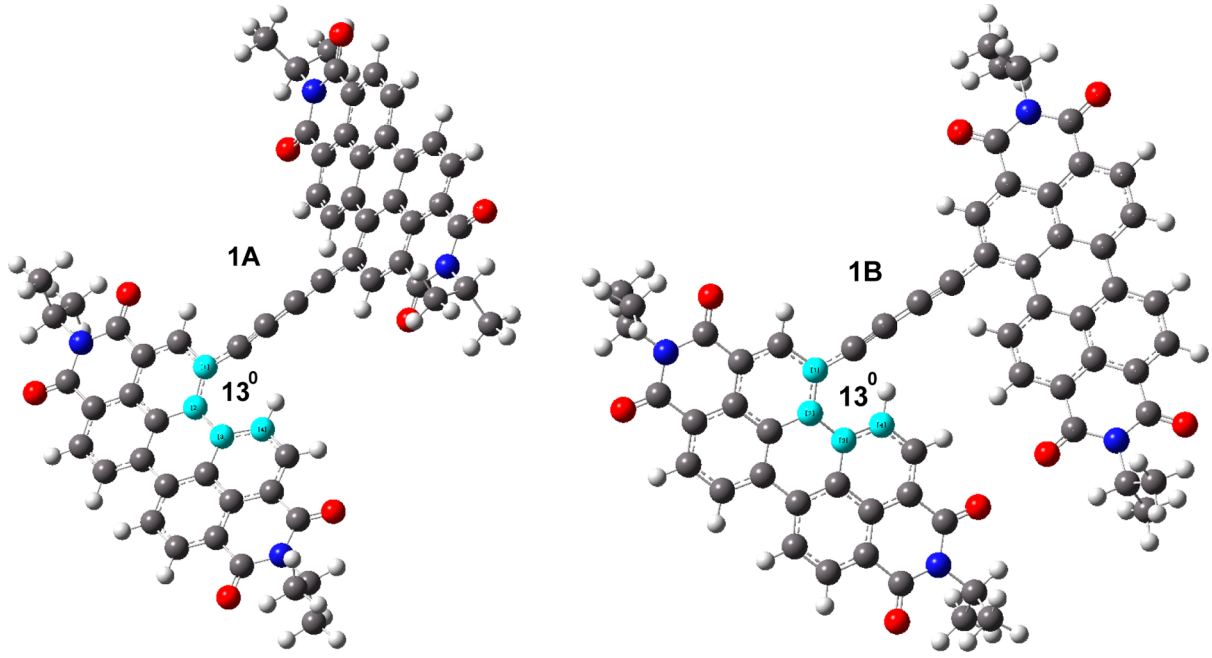

Figure 10. Optimized ground state geometry of **1** (DFT, B3LYP/6-31G(d)) in a chloroform solvent continuum (PCM): transoid (**1A**, left) and cisoid (**1B**, right) conformations. The perylene core is twisted around its central six-member ring with a calculated internal dihedral angle of 13°.

PDI dimer **1** (Figure 9). At 300 K, the P2 proton appears as a pseudodoublet produced by two heavily overlapping broad singlets of equal intensity, manifesting a textbook example of a dynamic spin system that exists in the slow-to-intermediate exchange regime.[56,57,68] In this regime, the dynamic behavior of **1** can be rationally described by a two-state conformational equilibrium model with nearly equal population distributions at RT. The coalescence point (305 K for **1** and 310 K for **2**, Figures 9 and Supporting Information S18) refers to the temperature at which the peak separation is no longer resolved and indicates a crossover into the fast exchange regime. Beyond this point (>310 K), the system shifts completely into the fast exchange mode, and the PDI conformational dynamics becomes too fast to be resolved into multiple components.

dx.doi.org/10.1021/jo401348w | J. Org. Chem. 2013, 78, 8634−8644

As a result, the P2 proton becomes a well-defined ensemble-average singlet, in complete accordance with its structural positioning within the molecular framework of **1**. In addition, at slightly elevated temperatures (320 − 330 K), the P11 proton (δ 8.82−8.79, Figure 8) becomes progressively better resolved as a doublet, exhibiting a scalar coupling of 8.0 Hz (typical value for 3-bond coupled aromatic protons)[69] with its P12 partner within the same spin system. In terms of more thorough analysis, the residual exchange-induced line broadening of the P2 proton can be conveniently used to estimate the rate constants (k_{ex}) and the activation barrier ($\Delta G‡$) for the observed conformational exchange (see the Experimental Section). The estimated activation energy for both PDI monomers (such as PDICCTMS) and dimers **1** and **2** was found to fall into the range of 13−17 kcal/mol (Supporting Information Figure S19, Table S3) and is in a good agreement with literature reported values for structurally related molecules that display chemical exchange dynamic behavior.[53,59,67,70−76]

On the basis of X-ray crystallographic and DFT studies, several recent reports have indicated that the bay region-directed substitution in PDI molecules brings about a substantial out-of-plane twist of the central six-member ring with dihedral angles ranging from 13.7° (1,7-disubstituted) to 37° (1,6,7,12-tetrasubstituted), depending on the nature of the substituents; on the other hand, photophysical data point toward the preservation of perylene core aromaticity.[26,35,62,77,78] Consistent with these observations, our DFT calculations of **1** in the lowest energy ground state geometry in chloroform solvent continuum (PCM) predicted the internal dihedral angle of 13° for both transoid **1A** and cisoid **1B** conformations (Figure 10). As a result, it appears reasonable to assume that both 1-hexylheptyl-incorporating PDI monomers and dimers (**1** and **2**) may be structurally predisposed to undergo the observed dynamic perylene-centered conformational oscillations.

■ CONCLUSIONS

We have synthesized and thoroughly characterized two representative ladder-type acetylene-bridged perylenediimide (PDI) dimers bearing long 1-hexylheptyl solubilizing groups. Notably, NMR structural characterization becomes nontrivial in these dimeric PDI molecules because substantial observed ambiguities complicate the interpretation of traditionally acquired 1-D spectra. However, rational two-dimensional NMR approaches (^{1}H−^{1}H COSY, ^{1}H−^{13}C HSQC) along with high-level DFT calculations (GIAO/B3LYP/6-31G(d,p)/PCM, chloroform) can be readily applied to these PDI structures, producing quite definitive analytical characterization. Furthermore, the dynamic NMR experiments proved to be essential in unraveling the associated conformational dynamic phenomenon ($\Delta G‡$ = 13−17 kcal/mol), which became a primary cause of the observed ambiguities in conventional 1-D spectra. The described structural characterization methodology, based on the combination of experimental NMR and computational DFT approaches, can be used as a reliable guide toward understanding various structural phenomena in many classes of complex organic and organometallic molecules.

■ EXPERIMENTAL SECTION

General. Most synthetic manipulations were carried out under inert atmosphere (argon) using standard Schlenk techniques unless otherwise noted.[69] All solvents (ACS reagent grade) and reagents were purchased from commercial sources and used as received. When necessary, anhydrous solvents were obtained from a standard solvent purification system equipped with activated alumina columns. Model PDI compounds bearing ethylpropyl substituents were obtained from previous studies.[66]

Characterization and Instrumentation. The structures of synthesized perylenediimide monomeric synthons along with acetylene-bridged dimers **1** and **2** were confirmed by high-resolution ^{1}H and ^{13}C NMR spectroscopy and MALDI-TOF mass spectrometry (MALDI-MS). Mass spectra were acquired using a standard MALDI-TOF spectrometer. 1-D ^{1}H (500 MHz) and ^{13}C (125 MHz) and 2-D correlation (^{1}H−^{1}H COSY, ^{1}H−^{13}C HSQC) NMR spectra were recorded at 300 K on a 500 MHz spectrometer equipped with a cryoprobe. Variable-temperature (VT) NMR experiments were carried out in the 300−330 K range with 5 ± 0.1 K increments and a sample temperature equilibration time of 10 min. The acquired 1-D and 2-D NMR spectra were analyzed using MestReNova 8.1.1 and Sparky 3.114 software, respectively. All chemical shifts were referenced to the internal tetramethylsilane (TMS) standard (δ 0.0 ppm), and splitting patterns were assigned as s (singlet), d (doublet), t (triplet), and m (multiplet). NMR line shape analysis was performed using Bruker TopSpin 2.1 software. The conformational exchange rate constants (k_{ex}) were calculated from the line shape broadening deconvolution of an uncoupled aromatic proton (P2) in the 310−330 K temperature range (fast exchange regime) assuming a two-state, equal population exchange model and using the following equation:[57,68]

$$k_{ex} = \frac{\pi(\nu_A - \nu_B)^2}{2(LW_{AB} - LW_{REF})}$$

where: (ν_A-ν_B) is the exchangeable uncoupled proton peak (P2) separation (in Hz) measured at 300 K (slow exchange regime); LW_{AB} is a line width (fwhm, in Hz) of the uncoupled exchangeable proton peak (P2) at a given temperature; LW_{REF} is the line width (fwhm, in Hz) of a reference nonexchangeable proton peak (TMS) at a given temperature. The activation energy ($\Delta G‡$) for the conformational exchange was estimated from the Arrhenius analysis ($\ln(k_{ex})$ vs $1/T$; see the Supporting Information).

DFT Calculations. DFT calculations were performed using the Gaussian 09 software package[79] and the computational resource of the Ohio Supercomputer Center. ^{1}H NMR DFT calculations were performed on the ground state optimized geometry molecules at the B3LYP/6-31G(d) level.[62,66,80] For the geometry optimization calculations, Cartesian coordinates were used, and no symmetry restrictions were applied. The polarizable continuum model (PCM) was used to simulate the effects of the chloroform solvent environment. To decrease the computational cost for the calculations of PDI dimer **1**, the long hexyl alkyl chains were substituted with methyl groups. Preliminary results showed that inclusion of the long alkyl chains did not affect the perylene core optimized geometry The rigid scan of the one-dimensional potential energy surface in a gas phase was performed using the B3LYP functional and 6-31G(d) basis set with a dihedral angle formed by diacetylene bridge as a variable. Two conformational minima (**1A** and **1B**) in the potential energy surface were found, followed by the optimization of the ground state energy using the B3LYP functional and 6-31G(d) basis set in a chloroform solvent

dx.doi.org/10.1021/jo401348w | J. Org. Chem. 2013, 78, 8634−8644

continuum (PCM) (Supporting Information Figure S16). Frequency calculations were performed on all optimized structures to ensure that these geometries correspond to local minima. ^{1}H NMR chemical shifts were calculated using the gauge-invariant atomic orbital (GIAO) method, B3LYP functional, and 6-31G(d,p) basis set in a chloroform solvent continuum (PCM).[60,61,81] In the case of PDI dimer **1**, ^{1}H NMR chemical shifts were calculated for both conformational minima, **1A** and **1B**. The obtained two sets of chemical shifts were averaged due to the negligible energy barrier of rotation between **1A** and **1B** (Supporting Information Table S2). ^{1}H NMR spectra were visualized using GaussView 5. The resulting chemical shifts were referenced to the shielding constant of tetramethylsilane (TMS) calculated at the same level of theory in a chloroform solvent continuum (PCM).

Synthesis and Characterization. The monomeric PDI synthons were synthesized via modified literature procedures; the representative synthetic scheme is demonstrated in Supporting Information Figure S1.[26,64] All synthesized monomeric PDI synthons produced satisfactory analytical characterization data that were found to be consistent with reported values. In general, symmetric 1-hexylheptylamine was obtained via a facile reductive amination of commercially available dihexylketone in the presence of $NaBH_3CN$. In the next step, 1-hexylheptylamine was condensed under ambient conditions with commercially available 3,4,9,10-perylene-tetracarboxylic dianhydride to obtain the corresponding perylenediimide (PDI) in a nearly quantitative yield. PDI was then selectively brominated in the 1-position of its bay region with elemental Br_2 to afford 1-bromo-perylenediimide (PDIBr). Even though the formation of PDIBr is most favorable under the employed reaction conditions, this reaction can be considered as a major yield-limiting step in which PDIBr is typically isolated in ∼50% yield due to competing polybromination side reactions. In the next step, PDIBr was Sonogashira cross-coupled with trimethylsilylacetylene (TMSA) to give the desired monomeric synthon PDICCTMS.[82,83] Subsequently, PDICCTMS was used as a departure point to gain access to target PDI dimers **1** and **2** (Supporting Information Figure S1). In general, PDI dimer **2** ($[PDI]_2CC$) was obtained in a two-step fashion via mild deprotection of PDICCTMS with K_2CO_3 to obtain PDICCH in a quantitative yield, which in turn was Sonogashira cross-coupled with excess PDIBr. On the other hand, PDI dimer **1** ($[PDICC]_2$) was obtained via a one-pot CuI-mediated, Pd-free simultaneous deprotection/homocoupling of PDICCTMS in DMF in the presence of atmospheric oxygen and represents a significant improvement over the previously reported methodology.[26,84,85] The detailed experimental procedures for the synthesis of PDI dimers **1** and **2** are provided below.

*Bis[1-ethynyl-N,N′-bis(1-hexylheptyl)-perylene-3,4:9,10-tetracarboxylic Diimide] ($[PDICC]_2$, **1**).* A 0.4 g (0.47 mmol) portion of PDICCTMS was dispersed in 100 mL of *N*,*N*-dimethylformamide upon sonication, followed by the addition of 0.19 g (1.0 mmol) of CuI. The reaction mixture was stirred at 80 °C for 24 h under ambient atmosphere in an open-neck flask. The reaction completion was confirmed by UV/vis spectroscopy. After cooling to RT, the reaction mixture was gently poured into water, and the obtained black precipitate was filtered off, redissolved in $CHCl_3$, washed with water and brine, and then dried over Na_2SO_4 (anh.). After the solvent removal under vacuum, the obtained solid was recrystallized at least three times from dichloromethane/methanol (1:3) via liquid diffusion to afford analytically pure dark red solid in 70% yield (0.25 g). MALDI-MS: m/z = 1557.4 ($[M + H]^+$). ^{1}H NMR (500 MHz, $CDCl_3$, 300 K): 10.10 (2H, d, J = 8.1 Hz); 8.96−8.92 (2H, m); 8.82−8.79 (2H, m); 8.74−8.66 (8H, m); 5.23−5.15 (4H, m); 2.30−2.21 (8H, m); 1.90−1.83 (8H, m); 1.38−1.21 (64H, m); 0.84 (12H, t, J = 6.9 Hz); 0.81 (12H, t, J = 6.9 Hz). ^{13}C NMR (125 MHz, $CDCl_3$, 300 K): 164.68; 164.38; 164.21; 163.72; 163.66; 163.32; 163.12; 162.52; 139.25; 138.58; 136.54; 134.61; 133.62; 132.28; 131.93; 131.54; 131.18; 130.79; 129.15; 129.07; 127.22; 126.89; 126.55; 124.85; 124.15; 123.69; 123.38; 122.99; 122.31; 117.70; 86.65; 82.73; 54.98; 54.79; 32.33; 31.78; 31.75; 29.23; 29.22; 26.92; 22.61; 22.59; 14.07; 14.05.

*1,1′-Ethynyl-bis[N,N′-bis(1-hexylheptyl)-perylene-3,4:9,10-tetracarboxylic Diimide] ($[PDI]_2CC$, **2**).* A 0.36 g (0.439 mmol) portion of PDIBr was dissolved in 300 mL of THF (anh.), and 7 mL of diisopropylamine (anh.) was added to the solution. The reaction mixture was degassed for 30 min with argon, and 0.02 g (0.105 mmol) of CuI and 0.169 g (0.024 mmol) of $Pd(PPh_3)_2Cl_2$ were added. The solution was heated to 80 °C, and 0.27 g (0.366 mmol) of PDICCH in 200 mL of argon saturated THF (anh.) was added dropwise over a period of 24 h. Once the addition was complete, the reaction mixture was stirred for 2 h. After cooling to RT, the solvent was removed under vacuum to afford the crude product as a dark purple solid. The crude product was purified by flash column chromatography on silica gel (hexane/dichloromethane =1:1). The solvent was removed under vacuum, and the product was recrystallized at least three times from $CHCl_3$/methanol (1:4) via liquid diffusion, resulting in an analytically pure dark red solid in 28% yield (0.155 g). MALDI-MS: m/z = 1533.54 ($[M + H]^+$).^{1}H NMR (500 MHz, $CDCl_3$, 300 K): 10.27 (2H, s); 9.01−8.97 (2H, m); 8.78−8.66 (10H, m); 5.25−5.16 (4H, m); 2.31−2.19 (8H, m); 1.92−1.86 (8H, m); 1.36−1.20 (64H, m); 0.84 (12H, t, J = 7.0 Hz); 0.81 (12H, t, J = 12.0 Hz). ^{13}C NMR (125 MHz, $CDCl_3$, 300 K): 164.68; 164.49; 164.25; 163.81; 163.59; 163.39; 163.14; 162.67; 138.13; 137.53; 135.32; 134.76; 134.01; 133.80; 132.26; 131.70; 131.50; 130.99; 129.27; 129.07; 127.47; 126.97; 126.74; 124.67; 124.19; 123.84; 123.42; 122.99; 122.63; 118.74; 99.39; 55.03; 54.79; 32.34; 31.78; 31.74; 29.24; 29.22; 26.95; 26.91; 22.62; 22.59; 14.07; 14.04.

■ ASSOCIATED CONTENT

Supporting Information

Representative synthetic scheme; 1-D ^{13}C NMR spectra of PDICCTMS and dimers **1** and **2**; assigned 1-D ^{1}H, 2-D ^{1}H−^{1}H COSY and ^{1}H−^{13}C HSQC NMR spectra of all related PDI monomers and dimer **2**; DFT calculated 1-D ^{1}H NMR spectrum of PDICCTMS; temperature-dependent 1-D ^{1}H NMR spectra of PDICCTMS and dimer **2**; conformational exchange kinetic analysis data; redundant coordinates with dihedral angle formed by diacetylene bridge as a variable for 1-D potential energy scan of **1** in gas phase; summary of 1-D potential surface scan for dimer **1**; ground state optimized geometry for ^{1}H NMR DFT GIAO calculations (Cartesian coordinates). This material is available free of charge via the Internet at http://pubs.acs.org.

■ AUTHOR INFORMATION

Corresponding Author

*Phone: (419) 372-7513. Fax: (419) 372-9809. E-mail: castell@bgsu.edu.

Present Address

[#]Department of Chemistry, North Carolina State University, Raleigh, NC 27695-8204. Phone: (919) 515-3021; Fax: (919) 515-8909; E-mail: fncastel@ncsu.edu.

Author Contributions

[§]M.M. and V.P. contributed equally to this work.

Notes

The authors declare no competing financial interest.

■ ACKNOWLEDGMENTS

This work was supported by DARPA (N66001-10-1-4059). The authors are grateful to Dr. Nataliya Popovych (Genentech, Inc.), Dr. Catherine E. McCusker, Prof. Massimo Olivucci, Dr. Samer Gozem, Dr. D. Y. Chen, Dr. Barry C. Pemberton (BGSU), and Dr. Vivekanandan Subramanian (University of Michigan) for their invaluable assistance with the analysis of NMR data and DFT calculations. We thank Prof. Ioannis Gelis (University of South Florida), Dr. Manoj K. Pandey and Dr. Janarthanan Krishnamoorthy (University of Michigan), Dr. Hyounsoo Uh, Dr. Papatya C. Sevinc, and Dr. Joseph C. Deaton (BGSU) for helpful discussions.

■ REFERENCES

(1) Langhals, H. *Helv. Chim. Acta* **2005**, *88*, 1309−1343.
(2) Wurthner, F. *Chem. Commun.* **2004**, 1564−1579.
(3) Castellano, F. N. *Dalton Trans.* **2012**, *41*, 8493−8501.
(4) Li, C.; Wonneberger, H. *Adv. Mater.* **2012**, *24*, 613−636.
(5) Weil, T.; Vosch, T.; Hofkens, J.; Peneva, K.; Mullen, K. *Angew. Chem., Int. Ed.* **2010**, *49*, 9068−9093.
(6) Zhan, X. W.; Facchetti, A.; Barlow, S.; Marks, T. J.; Ratner, M. A.; Wasielewski, M. R.; Marder, S. R. *Adv. Mater.* **2011**, *23*, 268−284.
(7) Rachford, A. A.; Goeb, S.; Castellano, F. N. *J. Am. Chem. Soc.* **2008**, *130*, 2766−2767.
(8) Danilov, E. O.; Rachford, A. A.; Goeb, S.; Castellano, F. N. *J. Phys. Chem. A* **2009**, *113*, 5763−5768.
(9) Conron, S. M. M.; Shoer, L. E.; Smeigh, A. L.; Ricks, A. B.; Wasielewski, M. R. *J. Phys. Chem. B* **2013**, *117*, 2195−2204.
(10) Yoo, H.; Furumaki, S.; Yang, J.; Lee, J. E.; Chung, H.; Oba, T.; Kobayashi, H.; Rybtchinski, B.; Wilson, T. M.; Wasielewski, M. R.; Vacha, M.; Kim, D. *J. Phys. Chem. B* **2012**, *116*, 12878−12886.
(11) Brown, K. E.; Veldkamp, B. S.; Co, D. T.; Wasielewski, M. R. *J. Phys. Chem. Lett.* **2012**, *3*, 2362−2366.
(12) Supur, M.; Fukuzumi, S. *J. Phys. Chem. C* **2012**, *116*, 23274−23282.
(13) Diacon, A.; Rusen, E.; Mocanu, A.; Hudhomme, P.; Cincu, C. *Langmuir* **2011**, *27*, 7464−7470.
(14) Yang, S. K.; Shi, X. H.; Park, S.; Doganay, S.; Ha, T.; Zimmerman, S. C. *J. Am. Chem. Soc.* **2011**, *133*, 9964−9967.
(15) Costa, R. D.; Cespedes-Guirao, F. J.; Bolink, H. J.; Fernandez-Lazaro, F.; Sastre-Santos, A.; Orti, E.; Gierschner, J. *J. Phys. Chem. C* **2009**, *113*, 19292−19297.
(16) Ribeiro, T.; Baleizao, C.; Farinha, J. P. S. *J. Phys. Chem. C* **2009**, *113*, 18082−18090.
(17) Briseno, A. L.; Mannsfeld, S. C. B.; Reese, C.; Hancock, J. M.; Xiong, Y.; Jenekhe, S. A.; Bao, Z.; Xia, Y. N. *Nano Lett.* **2007**, *7*, 2847−2853.
(18) Vura-Weis, J.; Ratner, M. A.; Wasielewski, M. R. *J. Am. Chem. Soc.* **2010**, *132*, 1738−1739.
(19) Baffreau, J.; Leroy-Lhez, S.; Hudhomme, P.; Groeneveld, M. M.; van Stokkum, I. H. M.; Williams, R. M. *J. Phys. Chem. A* **2006**, *110*, 13123−13125.
(20) Jimenez, A. J.; Grimm, B.; Gunderson, V. L.; Vagnini, M. T.; Calderon, S. K.; Rodriguez-Morgade, M. S.; Wasielewski, M. R.; Guldi, D. M.; Torres, T. *Chem.—Eur. J.* **2011**, *17*, 5024−5032.
(21) Baffreau, J.; Leroy-Lhez, S.; Van Anh, N.; Williams, R. M.; Hudhomme, P. *Chem.—Eur. J.* **2008**, *14*, 4974−4992.
(22) Singh-Rachford, T. N.; Nayak, A.; Muro-Small, M. L.; Goeb, S.; Therien, M. J.; Castellano, F. N. *J. Am. Chem. Soc.* **2010**, *132*, 14203−14211.
(23) Mete, E.; Uner, D.; Cakmak, M.; Gulseren, O.; Ellialtoglu, S. *J. Phys. Chem. C* **2007**, *111*, 7539−7547.
(24) Jaggi, M.; Blum, C.; Marti, B. S.; Liu, S. X.; Leutwyler, S.; Decurtins, S. *Org. Lett.* **2010**, *12*, 1344−1347.
(25) Oh, J. H.; Sun, Y. S.; Schmidt, R.; Toney, M. F.; Nordlund, D.; Konemann, M.; Wurthner, F.; Bao, Z. A. *Chem. Mater.* **2009**, *21*, 5508−5518.
(26) Yan, Q. F.; Zhao, D. H. *Org. Lett.* **2009**, *11*, 3426−3429.
(27) Sanchez, R. S.; Gras-Charles, R.; Bourdelande, J. L.; Guirado, G.; Hernando, J. *J. Phys. Chem. C* **2012**, *116*, 7164−7172.
(28) Gomez, R.; Seoane, C.; Segura, J. L. *J. Org. Chem.* **2010**, *75*, 5099−5108.
(29) Fron, E.; Deres, A.; Rocha, S.; Zhou, G.; Mullen, K.; De Schryver, F. C.; Sliwa, M.; Uji-i, H.; Hofkens, J.; Vosch, T. *J. Phys. Chem. B* **2010**, *114*, 1277−1286.
(30) Wilson, T. M.; Tauber, M. J.; Wasielewski, M. R. *J. Am. Chem. Soc.* **2009**, *131*, 8952−8957.
(31) Rodriguez-Morgade, M. S.; Torres, T.; Atienza-Castellanos, C.; Guldi, D. M. *J. Am. Chem. Soc.* **2006**, *128*, 15145−15154.
(32) Seitz, W.; Jimenez, A. J.; Carbonell, E.; Grimm, B.; Rodriguez-Morgade, M. S.; Guldi, D. M.; Torres, T. *Chem. Commun.* **2010**, *46*, 127−129.
(33) Albert-Seifried, S.; Finlayson, C. E.; Laquai, F.; Friend, R. H.; Swager, T. M.; Kouwer, P. H. J.; Juricek, M.; Kitto, H. J.; Valster, S.; Nolte, R. J. M.; Rowan, A. E. *Chem.—Eur. J.* **2010**, *16*, 10021−10029.
(34) Keerthi, A.; Valiyaveettil, S. *J. Phys. Chem. B* **2012**, *116*, 4603−4614.
(35) Wurthner, F.; Stepanenko, V.; Chen, Z. J.; Saha-Moller, C. R.; Kocher, N.; Stalke, D. *J. Org. Chem.* **2004**, *69*, 7933−7939.
(36) Sivalmurugan, V.; Kazlauskas, K.; Jursenas, S.; Gruodis, A.; Simokaitiene, J.; Grazulevicius, J. V.; Valiyaveettil, S. *J. Phys. Chem. B* **2010**, *114*, 1782−1789.
(37) Dubey, R. K.; Efimov, A.; Lemmetyinen, H. *Chem. Mater.* **2011**, *23*, 778−788.
(38) Seki, T.; Asano, A.; Seki, S.; Kikkawa, Y.; Murayama, H.; Karatsu, T.; Kitamura, A.; Yagai, S. *Chem.—Eur. J.* **2011**, *17*, 3598−3608.
(39) Gorl, D.; Zhang, X.; Wurthner, F. *Angew. Chem., Int. Ed.* **2012**, *51*, 6328−6348.
(40) Li, X. Y.; Sinks, L. E.; Rybtchinski, B.; Wasielewski, M. R. *J. Am. Chem. Soc.* **2004**, *126*, 10810−10811.
(41) Cao, X. Q.; Wu, Y. S.; Fu, H. B.; Yao, J. N. *J. Phys. Chem. Lett.* **2011**, *2*, 2163−2167.
(42) Colby, K. A.; Bardeen, C. J. *J. Phys. Chem. A* **2011**, *115*, 7574−7581.
(43) van der Boom, T.; Hayes, R. T.; Zhao, Y. Y.; Bushard, P. J.; Weiss, E. A.; Wasielewski, M. R. *J. Am. Chem. Soc.* **2002**, *124*, 9582−9590.
(44) El-Khouly, M. E.; Jaggi, M.; Schmid, B.; Blum, C.; Liu, S. X.; Decurtins, S.; Ohkubo, K.; Fukuzumi, S. *J. Phys. Chem. C* **2011**, *115*, 8325−8334.
(45) Nolde, F.; Pisula, W.; Muller, S.; Kohl, C.; Mullen, K. *Chem. Mater.* **2006**, *18*, 3715−3725.
(46) Shao, C.; Stolte, M.; Wurthner, F. *Angew. Chem., Int. Ed.* **2013**, *52*, 7482−7486.
(47) Claridge, T. D. W. *High-Resolution NMR Techniques in Organic Chemistry*; Elsevier: New York, 2000.
(48) Hu, J. J.; Xu, T. W.; Cheng, Y. Y. *Chem. Rev.* **2012**, *112*, 3856−3891.
(49) Pastor, A.; Martinez-Viviente, E. *Coord. Chem. Rev.* **2008**, *252*, 2314−2345.
(50) Myahkostupov, M.; Castellano, F. N. *Inorg. Chem.* **2011**, *50*, 9714−9727.
(51) Popovych, N.; Tzeng, S. R.; Tonelli, M.; Ebright, R. H.; Kalodimos, C. G. *Proc. Natl. Acad. Sci. U.S.A.* **2009**, *106*, 6927−6932.

(52) Friebolin, H. *Basic One- and Two-Dimensional NMR Spectroscopy*; Wiley-VCH: New York, 2010.
(53) Perrin, C. L.; Dwyer, T. J. *Chem. Rev.* **1990**, *90*, 935−967.
(54) Popovych, N.; Sun, S. J.; Ebright, R. H.; Kalodimos, C. G. *Nat. Struct. Mol. Biol.* **2006**, *13*, 831−838.
(55) Tzeng, S. R.; Kalodimos, C. G. *Curr. Opin. Struct. Biol.* **2011**, *21*, 62−67.
(56) Palmer, A. G. *Chem. Rev.* **2004**, *104*, 3623−3640.
(57) Sandstrom, J. *Dynamic NMR Spectroscopy*; Academic Press: New York, 1982.
(58) Rinnenthal, J.; Buck, J.; Ferner, J.; Wacker, A.; Furtig, B.; Schwalbe, H. *Acc. Chem. Res.* **2011**, *44*, 1292−1301.
(59) Casarini, D.; Lunazzi, L.; Mazzanti, A. *Eur. J. Org. Chem.* **2010**, 2035−2056.
(60) Bagno, A.; Rastrelli, F.; Saielli, G. *Chem.—Eur. J.* **2006**, *12*, 5514−5525.
(61) Helgaker, T.; Jaszunski, M.; Kenneth, R. *Chem. Rev.* **1999**, *99*, 293−352.
(62) Liang, B.; Zhang, Y.; Wang, Y.; Xu, W.; Li, X. *J. Mol. Struct.* **2009**, *917*, 133−141.
(63) Shi, Y.; Wu, H. X.; Xue, L.; Li, X. Y. *J. Colloid Interface Sci.* **2012**, *365*, 172−177.
(64) Huang, Y. W.; Hu, J. C.; Kuang, W. F.; Wei, Z. X.; Faul, C. F. J. *Chem. Commun.* **2011**, *47*, 5554−5556.
(65) Shao, C.; Grune, M.; Stolte, M.; Wurthner, F. *Chem.—Eur. J.* **2012**, *18*, 13665−13677.
(66) Prusakova, V.; McCusker, C. E.; Castellano, F. N. *Inorg. Chem.* **2012**, *51*, 8589−8598.
(67) Osswald, P.; Wurthner, F. *Chem.—Eur. J.* **2007**, *13*, 7395−7409.
(68) Gasparro, F. P.; Kolodny, N. H. *J. Chem. Educ.* **1977**, *54*, 258-261.
(69) Furniss, B. S.; Hannaford, A. J.; Smith, P. W. G.; Tatchell, A. R. *Vogel's Textbook of Practical Organic Chemistry*; 5th ed.; Longman Group UK Ltd.: London, 1989.
(70) Eisenberg, D.; Filatov, A. S.; Jackson, E. A.; Rabinovitz, M.; Petrukhina, M. A.; Scott, L. T.; Shenhar, R. *J. Org. Chem.* **2008**, *73*, 6073−6078.
(71) Wang, Y.; Stretton, A. D.; McConnell, M. C.; Wood, P. A.; Parsons, S.; Henry, J. B.; Mount, A. R.; Galow, T. H. *J. Am. Chem. Soc.* **2007**, *129*, 13193−13200.
(72) Schwab, G.; Stern, D.; Stalke, D. *J. Org. Chem.* **2008**, *73*, 5242−5247.
(73) Toyota, S.; Makino, T. *Tetrahedron Lett.* **2003**, *44*, 7775−7778.
(74) Lunazzi, L.; Mancinelli, M.; Mazzanti, A. *J. Org. Chem.* **2008**, *73*, 2198−2205.
(75) Biali, S. E.; Rappoport, Z. *J. Org. Chem.* **1986**, *51*, 2245−2250.
(76) Paquette, L. A.; Wang, T. Z.; Luo, J. M.; Cottrell, C. E.; Clough, A. E.; Anderson, L. B. *J. Am. Chem. Soc.* **1990**, *112*, 239−253.
(77) Chen, Z. J.; Baumeister, U.; Tschierske, C.; Wurthner, F. *Chem.—Eur. J.* **2007**, *13*, 450−465.
(78) Chen, Z. J.; Debije, M. G.; Debaerdemaeker, T.; Osswald, P.; Wurthner, F. *ChemPhysChem* **2004**, *5*, 137−140.
(79) Frisch, M. J.; Trucks, G. W.; Schlegel, H. B.; Scuseria, G. E.; Robb, M. A.; Cheeseman, J. R.; Scalmani, G.; Barone, V.; Mennucci, B.; Petersson, G. A.; Nakatsuji, H.; Caricato, M.; Li, X.; Hratchian, H. P.; Izmaylov, A. F.; Bloino, J.; Zheng, G.; Sonnenberg, J. L.; Hada, M.; Ehara, M.; Toyota, K.; Fukuda, R.; Hasegawa, J.; Ishida, M.; Nakajima, T.; Honda, Y.; Kitao, O.; Nakai, H.; Vreven, T.; Montgomery, J. A., Jr.; Peralta, J. E.; Ogliaro, F.; Bearpark, M.; Heyd, J. J.; Brothers, E.; Kudin, K. N.; Staroverov, V. N.; Kobayashi, R.; Normand, J.; Raghavachari, K.; Rendell, A.; Burant, J. C.; Iyengar, S. S.; Tomasi, J.; Cossi, M.; Rega, N.; Millam, J. M.; Klene, M.; Knox, J. E.; Cross, J. B.; Bakken, V.; Adamo, C.; Jaramillo, J.; Gomperts, R.; Stratmann, R. E.; Yazyev, O.; Austin, A. J.; Cammi, R.; Pomelli, C.; Ochterski, J. W.; Martin, R. L.; Morokuma, K.; Zakrzewski, V. G.; Voth, G. A.; Salvador, P.; Dannenberg, J. J.; Dapprich, S.; Daniels, A. D.; Farkas, O.; Foresman, J. B.; Ortiz, J. V.; Cioslowski, J.; Fox, D. J. *Gaussian 09*, revision C.01; Gaussian, Inc.: Wallingford CT, 2010.
(80) Polyansky, D. E.; Danilov, E. O.; Castellano, F. N. *Inorg. Chem.* **2006**, *45*, 2370−2372.
(81) Wolinski, K.; Hinton, J. F.; Pulay, P. *J. Am. Chem. Soc.* **1990**, *112*, 8251−8260.
(82) Chinchilla, R.; Najera, C. *Chem. Rev.* **2007**, *107*, 874−922.
(83) de Meijere, A.; Diederich, F. *Metal-Catalyzed Cross-Coupling Reactions*; 2nd ed.; Wiley-VCH: New York, 2004.
(84) Nishihara, Y.; Ikegashira, K.; Hirabayashi, K.; Ando, J.; Mori, A.; Hiyama, T. *J. Org. Chem.* **2000**, *65*, 1780−1787.
(85) Liu, C.; Zhang, H.; Shi, W.; Lei, A. W. *Chem. Rev.* **2011**, *111*, 1780−1824.